First principles absorption spectra of Au nanoparticles: from quantum to classical

Samuel Hernandez[a*], Yantao Xia[b*], Vojtěch Vlček[a], Robert Boutelle[a], Roi Baer[c], Eran Rabani[d,e], Daniel Neuhauser[a]

[a] Department of Chemistry and Biochemistry, University of California, Los Angeles, California 90095, USA.; [b] Department of Chemical and Biomolecular Engineering, University of California, Los Angeles, California 90095, USA.; [c] Fritz Haber Center for Molecular Dynamics and Institute of Chemistry, The Hebrew University of Jerusalem, Jerusalem 9190401, Israel; [d] Department of Chemistry, University of California, Berkeley, California 94720, USA. [e] The Raymond and Beverly Sackler Center for Computational Molecular and Materials Science, Tel Aviv University, Tel Aviv 69978, Israel.

Abstract

Absorption cross-section spectra for gold nanoparticles were calculated using fully quantum Stochastic Density Functional Theory and a classical Finite-Difference Time Domain (FDTD) Maxwell solver. Spectral shifts were monitored as a function of size (1.3–3.1 nm) and shape (octahedron, cuboctahedron, and truncated cube). Even though the classical approach is forced to fit the quantum TDDFT at 3.1nm, at smaller sizes there is a significant deviation as the classical theory is unable to account for peak splitting and spectral blue shifts even after quantum spectral corrections. We attribute the failure of classical methods at predicting these features to quantum effects and low density of states in small nanoparticles. Classically, plasmon resonances are modeled as collective conduction electron excitations, but at small nanoparticle size these excitations transition to few or even individual conductive electron excitations, as indicated by our results.

Introduction

The unique physical and chemical properties of nanoparticles have generated intense academic and industrial interest, in hope that these properties, once well-understood, could be used for technological advances. nanoparticle materials exhibit physical and chemical properties very different from those of their bulk counterparts, often resulting from enhanced surface interactions or quantum effects [1]. For example, noble metal nanoparticles are drawing intense interest because of their ability to sustain localized surface-plasmon resonances (LSPRs) [2]. LSPRs are collective oscillations of surface conduction band electrons excited by an oscillating electric field, typically a photon. These oscillations enable strong absorption and scattering of subwavelength structures. Coupling of photons to conduction band electrons at metal interfaces improves efficiency for ultrafine sensing methods [3, 4], enhanced catalysis [5], energy-transfer [6, 7], and has enabled applications such as light concentrators in solar cells [8] and cancer therapies [9].

---

*These authors contributed equally to this work.

Experimental characterization of metallic nanoparticles is extremely difficult, since optical detection in the far-field is hampered by low signal to noise ratio due to low scattering and absorption intensities [10]. The LSPR peaks are further broadened and damped as the size of the particle decreases below the electron mean free path (40 nm for gold [11]). Finally, the spectral properties are strongly coupled to the stoichiometry, size, shape, and surrounding medium [2, 12, 13] making an *a priori* prediction difficult. The difficulty in observing broad, weak LSPR signals has led to conflicting results from experiments involving quantum-sized plasmonic particles, with multiple reports of LSPR redshifts or blueshifts as the size is reduced [14, 15].

Theoretical investigations often rely on classical methods, such as Mie Theory [16] and Finite-Difference Time-Domain (FDTD) Maxwell Solvers [17] which however inherently do not capture quantum effects important at scales of few nm. Size-dependent electron scattering terms have been included in the classical approaches, but the use of these correction results in predictions with redshifts and imperceptible plasmon resonances at small size scales [18] that conflict with experimental findings [19–21]. Additionally, the classical models assume a density of states (DOS) sufficiently populated in the Fermi level such that the LSPRs are a collective electron oscillation. This picture is however challenged by experiments, which suggest that small clusters (below 3nm) exhibit nonmetallic character so that with decreasing size, discrete peaks appear in their optical spectra [19, 22].

In this work fully first-principles quantum methods such as time-dependent density functional theory (TDDFT) are used to investigate the transition to the quantum regime of photo absorption cross sections in gold nanoparticles. Observation of the transition in gold requires applying TD-DFT to large nanoparticles including several hundreds of atoms. For this, we employ the recently developed stochastic approach to electronic structure [23–25] and in particular the stochastic TDDFT (sTDDFT) approach [26], which allows linear-scaling effort with respect to system size. We studied a range of stable [27, 28] closed-shell nanoparticles containing between 44 and 344 atoms, corresponding to diameters of 1.34 to 3.12 nm. By comparing with classical Maxwell simulations, we find that systems having less than ∼200 atoms exhibit strong quantum signatures (appearance of new absorption maxima and peak splitting) which depend on shape of the nanoparticle and are missing in the FDTD results.

Theory

In this section, we begin by reviewing the theory of absorption of light by small particles, in both the quantum-mechanical and classical picture. Next, we present the respective implementation of the quantum and classical theories in computational chemistry, namely the stochastic TDDFT and the FDTD Maxwell Equations, and explain their merits and limitations.

Within the linear response approach, the photo absorption cross section is given by

$$\sigma(\omega) = \frac{e^2}{3\epsilon_0 c}\omega \int \mathbf{r} \cdot \chi(\mathbf{r}, \mathbf{r}', \omega) \cdot \mathbf{r}' \, d\mathbf{r}d\mathbf{r}', \tag{1}$$

where polarizability relates induced charge density δn and external perturbing poten-

tial δv:

$$\chi \left(\mathbf{r}, \mathbf{r}', t - t' \right) = \frac{\delta n \left(\mathbf{r}, t \right)}{\delta v \left(\mathbf{r}', t' \right)}. \tag{2}$$

The external perturbing potential takes form of a dipole that perturbs the system instantaneously at $t = 0$:

$$\delta v \left(\mathbf{r}, t \right) = \gamma r_i \delta \left(t \right) \tag{3}$$

where $r_i = x, y$ or z is one of the components of the Cartesian vector $\mathbf{r}$. Here, the particles we consider are symmetric so the absorption spectrum will be identical for all polarization directions. Therefore, with no loss of generality $i = 1$ and $r_i = x$ below.

The impulsive perturbation excites the system at all frequencies. The perturbed system is propagated in time, and the induced dipole moment signal is computed:

$$\mu_i(t) = \int r_i \delta n(\mathbf{r}, t) d\mathbf{r}. \tag{4}$$

Finally the absorption cross section $\sigma \left(\omega \right) = \sum_{i=x,y,z} \sigma_{ii} \left(\omega \right)$ is obtained from:

$$\sigma_{ii}(\omega) = \frac{e^2}{\epsilon_0 c} \omega \int_0^\infty dt e^{i\omega t} \mu_i \left(t \right). \tag{5}$$

We compute the time-evolution of the induced charge density $\delta n \left(\mathbf{r}, t \right)$ using first-principles time-dependent DFT, starting from the ground state Kohn-Sham (KS) system with Hamiltonian (in atomic units)

$$H \left[n \right] = -\frac{1}{2} \nabla^2 + v_{ext} \left(\mathbf{r} \right) + v_H \left[n \right] \left(\mathbf{r} \right) + v_{xc} \left(n \left(\mathbf{r} \right) \right), \tag{6}$$

where $v_{ext} \left(\mathbf{r} \right)$ is the external (nuclear) potential energy and $v_H \left[n \right] \left(\mathbf{r} \right) = \int n \left(\mathbf{r}' \right) \left| \mathbf{r} - \mathbf{r}' \right|^{-1} d\mathbf{r}'$ is the Hartree potential. The last term $v_{xc} \left(n \right)$ is the exchange-correlation potential in the local density approximation (LDA)[29].

The Hamiltonian is associated with a complete set of eigenstates $\{ \phi_j \left(\mathbf{r} \right) \}$ and corresponding eigenvalues $\{ \varepsilon_j \}$ ($j = 1, 2, \dots$ is the state index) which are used as initial states of the system at time $t = 0$ when the perturbation of Eq. (3) is applied. At this moment and for subsequent times $t \geq 0$ the total density is a weighted sum of the instantaneous state densities $\left| \phi_j \left(\mathbf{r}, t \right) \right|^2$

$$n \left(\mathbf{r}, t \right) = 2 \sum_j f_\beta \left(\varepsilon_j, \mu \right) \left| \phi_j \left(\mathbf{r}, t \right) \right|^2, \tag{7}$$

where f_β is the Fermi-Dirac occupation function depending on the temperature $1/\beta$ and chemical potential μ at time $t = 0$ (the factor of 2 is due to spin degeneracy). Simultaneously, the states $\phi_j \left(\mathbf{r}, t \right)$ evolve in time according to the time-dependent KS equation

$$i \frac{\partial \phi_j \left(\mathbf{r}, t \right)}{\partial t} = \left(H \left[n \left(t \right) \right] + \delta v \left(\mathbf{r}, t \right) \right) \phi_j \left(\mathbf{r}, t \right), \tag{8}$$

3

where the Hamiltonian changes with time due to its implicit dependence on the time-evolving density. A general exchange-correlation potential would include memory effects and would therefore be non-local in time. But here we resort to adiabatic local density approximation (ALDA), in which $v_{xc}(n(\mathbf{r}, t)$ is a function of $n(\mathbf{r}, t)$ only.

The LDA and ALDA calculations are performed using Troullier-Martins pseudopotentials on a real-space grid with N_g points and a spacing of 0.6 a_0, sufficient to converge the occupied eigenvalues to within 10 meV. The real-time propagation in its canonical form, i.e., propagating each individual KS according to Eq. (8) is numerically demanding because of the quadratic scaling involved, namely $O(NN_g)$ with a large prefactor where N is the number of occupied states. In addition, there is of course the cost of obtaining the ground state. We used deterministic DFT which generally scales, depending on the method, as $O(N^2) - O(N^3)$; the DFT was more expensive that the stochastic TDDFT method. An alternative to the usual DFT would have been stochastic DFT,[23] which would have been faster for the largest clusters.

To lower the TDDFT cost, we recently developed a stochastic framework for TDDFT with (sub)linear scaling[26]. Instead of using a set of all N eigenstates $\{\phi_j\}$, the occupied subspace is represented by $|\zeta\rangle$ obtained as random linear combination:

$$|\zeta\rangle = \sum_j^N e^{i\theta_j} \sqrt{f_\beta(\varepsilon_j, \mu)} |\phi_j\rangle \tag{9}$$

where j is a state index and $\theta_j \in [0, 2\pi]$ is a random phase. Each ζ is a stochastic vector created using a distinct set of random phases $\{\theta_j\}$. All required quantities are expressed using a stochastic average over N_ζ vectors denoted $\{\cdots\}_\zeta$. For instance, the charge density is

$$n^s(\mathbf{r}) = \left\{ |\zeta(\mathbf{r})|^2 \right\}_\zeta. \tag{10}$$

Since the Hamiltonian in Eq. (6) is a functional of the density, it also has a stochastic representation denoted H^s.

Finally, the stochastic orbitals $|\zeta\rangle$ are propagated using a Trotter decomposition corresponding to the adiabatic stochastic time-dependent KS equations:

$$i \frac{\partial \zeta(\mathbf{r}, t)}{\partial t} = (H^s[n(t)] + \delta v(\mathbf{r}, t)) \zeta(\mathbf{r}, t), \tag{11}$$

After each propagation step $\delta\tau$, the charge density is evaluated by

$$n^s(\mathbf{r}, t) = \left\{ |\zeta(\mathbf{r}, t)|^2 \right\}_\zeta, \tag{12}$$

and the induced dipole $\mu_i(t)$ is calculated from Eq. (4). The stochastic charge density is then used to construct H^s and the TD procedure is repeated for the next time step $\delta\tau$, and the propagation continues for several femtoseconds. Finally, the absorption cross section σ is computed from the dipole signal $\mu_i(t)$ through Eq. (5).

The classical absorption spectrum is obtained from a finite-difference time-dependent (FDTD) propagation of the Maxwell Equations, using the MIT Electromagnetic Equation Propagation (MEEP) [17] open-source package. In FDTD, the metallic nanoparticle is modeled as polarizable material with complex dielectric permittivity
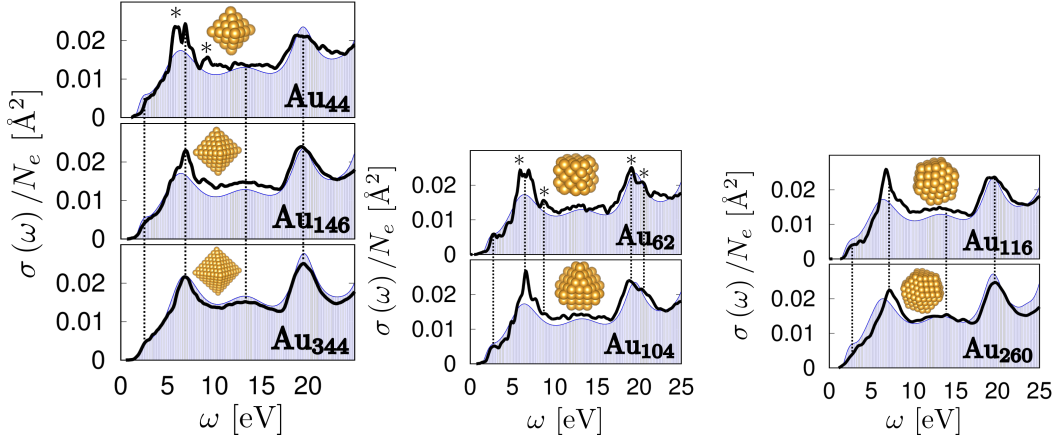
4

Figure 1. Photoabsorption cross-section spectra for Au octahedra (left panel), cubes (middle panel) and cuboctahedra (right panel). The TDDFT (black curve) and FDTD (blue-shaded are) results are superimposed. Vertical dashed lines show the position of the main peaks. The splittings of the main peaks in the low (5–10 eV) and medium (17–22 eV) frequency regions are indicated by stars (*). Note that the statistical errors in the stochastic TDDFT (employed for cluster sizes bigger than Au_{62}) are smaller than the line width so that the features in the small-cluster spectra are not artifacts.

given by

$$\epsilon(\omega) = \epsilon^D(\omega) + \epsilon^L(\omega). \tag{13}$$

Here, $\epsilon^D(\omega)$ is the intraband part, described by the Drude model:

$$\epsilon^D(\omega) = 1 - \frac{f_0 \omega_p^2}{\omega(\omega - i\Gamma_0)}, \tag{14}$$

where ω_p is the plasma frequency of gold and f_0, Γ_0 are the intraband oscillator strength and damping constant respectively. $\epsilon^L(\omega)$ is the interband part of the dielectric permittivity, modeled as a sum of K (typically $K = 2 - 10$) Lorentz-type terms,

$$\epsilon^L(\omega) = \sum_{j=1}^{K} \frac{f_j \omega_p^2}{\left(\omega_j^2 - \omega^2\right) + i\omega\Gamma_j}, \tag{15}$$

where ω_j, f_j and Γ_j^{-1} are, respectively, the j'th oscillator frequency, strength, and lifetime. We discuss below how all these parameters were determined.

TDDFT absorption spectra

We consider a set of nanoparticles with octahedral, truncated cube and cuboctahedral shapes with diameters ranging between 1.34 and 3.12 nm containing up to 3784 valence electrons. We use several closed shell systems that were previously determined to have stable shapes and stoichiometries, [27, 28] as summarized in Table 1 and shown in Fig. 1.

5

Table 1. Summary of the structures. Oct., Tr.Cb., and Cuboct. refers to octahedron, truncated cube, and cuboctahedrons, respectively.

nanoparticle	N_e	Size [nm]	Shape
Au_{44}	484	1.34	Oct.
Au_{146}	1606	2.23	Oct.
Au_{344}	3784	3.12	Oct.
Au_{62}	682	1.34	Tr.Cb.
Au_{104}	1144	1.64	Tr.Cb.
Au_{116}	1276	1.61	Cuboct.
Au_{147}	1617	2.23	Cuboct.

The time-dependent electron density was obtained with stochastic TDDFT for all systems except the smallest, Au_{44} and Au_{62}, where deterministic calculations were employed. The TDDFT time step was $\delta\tau = 0.03$ a.u. and for the stochastic calculations we used $N_\zeta = 400$ projected random vectors ζ. This value of N_ζ enables stable propagation up to 12 fs. The stochastic propagation is especially stable for this metallic system where the dipole is strongly damped.

The TDDFT optical absorption cross sections were calculated for each system and are shown in Fig. 1. With the exception of Au_{260}, all systems have their first absorption local maximum at 2.8 eV, a 0.4eV blue shift from values measured in n-heptane [30]. The presence of a polarizable medium (the n-heptane solvent) results in shifting the peaks to lower energies and explains, at least partially, the discrepancy between experiment and our calculations of nanoparticles in vacuum. While this peak is clearly found in the spectra of truncated cubes and cubooctahedra, its signature is much weaker for octahedra.

We discuss the spectral features in the three spectral regions, going from the larger to the smaller systems (c.f. Fig. 1):

(1) Intensity at lower frequencies (5 to 10 eV): For the two largest systems (Au_{344} and Au_{260}) only a single peak is observed (at 6.8 and 7.1 eV for the two systems, respectively). As the nanoparticle diameter decreases the peak is split in three (where the side bands are marked by stars). The small truncated cubes Au_{62} and Au_{104} always exhibit three maxima in this region. Note that except for the smallest systems (Au_{44} and Au_{62}), the central peak dominates this spectral region.

(2) The mid range (10 to 16 eV): The octahedral nanoparticles exhibit a splitting of a broad maximum found at 13.3 eV for Au_{344}. Spectra for other nanoparticle geometries show several local maxima.

(3) High frequencies (17 to 22 eV): Here, a single major peak is found, shifting to higher frequencies as the system size increases. Splitting is observed for truncated cubes (emphasized by stars above the corresponding peaks in the figure). Note that cuboctahedra do not exhibit the splitting as can be seen from comparison of Au_{104} and Au_{116} in the figure.

The transition from quantum to classical absorption

As the system size gets smaller, the spectra change. One manifestation is that the frequency spectrum becomes more refined, as mentioned above. This is manifested clearly already at the level of the time-dependent dipole moment per valence electron,
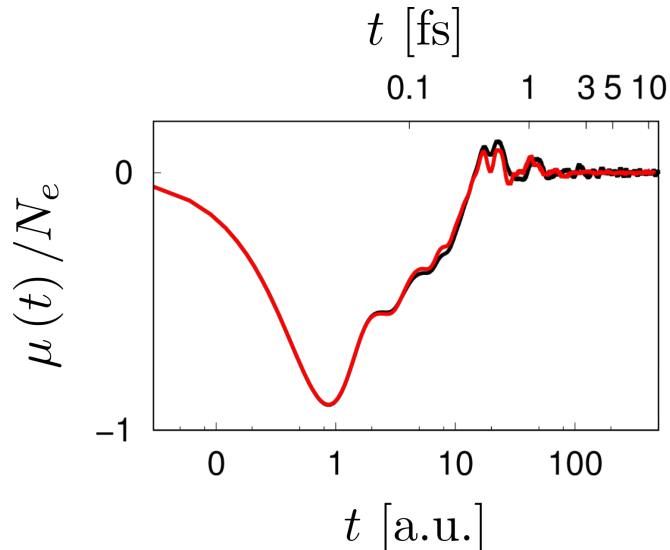
Figure 2. Induced dipole per valence electron as a function of time for the smallest and the largest systems investigated.

$\mu_x\left(t\right)/N_e$, (Eq. 4), shown in Fig. 2 for the largest and smallest systems investigated. At early times, the two $\mu_x\left(t\right)$ curves are almost indistinguishable and the difference in system size shows up at later times, where the large system's dipole decays faster.

The next stage is to compare to the classical spectrum. For this, we need to supply the K oscillators' parameters. Typically, they are fitted to experimentally measured real and imaginary optical dielectric functions of the modeled bulk gold [31, 32]. However, our goal is to focus on the transition from quantum to classical absorption for nanoparticles in the quantum regime, i.e., that are smaller than 3-5nm [33]. Therefore, we fitted the K oscillators' parameters to the TDDFT absorption cross-section for the *largest* gold nanoparticle (Au$_{344}$) and then use the same dielectric function for all FDTD (classical) calculations. The fit used a large frequency range, 0.5 to 25 eV, well above the 5.3eV work function of gold [34]. We used the Differential Evolution (DE) algorithm [35] to find oscillator parameters which minimize the following objective function:

$$\chi^2 = \int \left| \frac{\sigma_{\text{TDDFT}}\left(\omega\right) - \sigma_{\text{FDTD}}\left(\omega\right)}{\sigma_{\text{TDDFT}}\left(\omega\right)} \right| d\omega. \tag{16}$$

We found an optimal fit using $K = 6$ oscillators shown in the Table 2.

Comparing the classical and TDDFT spectra in Fig. 1 reveals that for all systems smaller than Au$_{344}$ the finer observed behavior is not captured well. Only the first peak at 2.8 eV is correctly found to be insensitive to system size and shape, in agreement with results from stochastic TDDFT calculations. For all systems, FDTD spectra is very smooth and show only three major peaks.

The first maximum shows slight size dependence, its position for Au$_{344}$ and Au$_{44}$ is shifted by 0.4 eV to lower frequencies for the smaller nanoparticle, but no splitting is observed. The position of other peaks in the FDTD spectra remains unchanged. Furthermore, TDDFT captures slight shape difference between Au$_{116}$ and Au$_{104}$ as symmetrical splitting of the peak at 19.7 eV, which is completely absent in the FDTD

7

Table 2. Values of the Lorentz-Drude model parameters. Values are given in eV. The plasma frequency was taken from Ref. [32] as 9.03 eV.

Oscillator	ω_j	f_j	Γ_j
0	0.000	1.234	0.000
1	0.523	0.000	1.735
2	4.000	2.479	5.506
3	12.921	1.980	7.467
4	18.831	2.405	3.223
5	25.568	20.000	3.325

results. We note that the lack of shape dependence in the FDTD spectra cannot be attributed to the coarseness of the real-space grid employed in the classical simulation since that was well converged even for the smallest system investigated (Au_{44}). Instead, we attribute the changes in the spectra to quantum signatures and decreased DOS population in the Fermi energy.

For small nanoparticle sizes, quantum confinement effects dominate the spectra and individual electronic states couple more strongly to the nanoparticle surface. Furthermore, broad spectral features break down to individual electronic transitions leading to multiple sharp maxima. Within the classical FDTD approach, the shape of the system is treated as homogeneous and isotropic polarizable continuum but its precise geometry (octahedron, cuboctahedron or truncated cube) has only negligible effect on the resulting absorption.

Summary and Conclusions

We used an FDTD Maxwell solver and our newly developed sTDDFT method to investigate the effect of size and shape on the absorption cross section of gold nanoparticles as large as 3nm. The sTDDFT calculated spectra show features that are consistent with the classical Maxwell theory as the system approaches the bulk limit. Moreover, the fine structure, significant in the small systems, agree with our a-priori expectation: in large particles where the properties are essentially metallic, the infinite number of states will result in a continuous, smooth absorption spectrum. As the systems become smaller, the finite number of states lead to discretization and splittings in the spectra. This is in line with experimental results where individual gold nanoparticles below 3 nm show reduction in the DOS of the Fermi level [22], and is reflected by the jagged nature of the spectrum for small clusters.

Based on these observations, we conclude that even when we force the classical methods to fit qualitatively the TDDFT optical properties of gold nanoparticles at 3 nm, it will lose the finer detail for smaller nanoparticles.

Our studies verify that stochastic TDDFT is a valid technique for calculating absorption cross-section of bulk-like gold nanoparticles. They also show that or particles smaller than 3 nm, fully quantum methods are required to predict the finer details of the absorption cross-section spectra.

Acknowledgments

References

[1] Dan Guo, Guoxin Xie, and Jianbin Luo. Mechanical properties of nanoparticles: basics and applications. *J. Phys. D: Appl. Phys.*, 47(1):013001, 2013.

[2] Katherine A Willets and Richard P Van Duyne. Localized surface plasmon resonance spectroscopy and sensing. *Annu. Rev. Phys. Chem.*, 58:267–297, 2007.

[3] Kathryn M Mayer and Jason H Hafner. Localized surface plasmon resonance sensors. *Chem. Rev.*, 111(6):3828–3857, 2011.

[4] Katrin Kneipp, Yang Wang, Harald Kneipp, Lev T Perelman, Irving Itzkan, Ramachandra R Dasari, and Michael S Feld. Single molecule detection using surface-enhanced raman scattering (sers). *Phys. Rev. Lett.*, 78(9):1667, 1997.

[5] Phillip Christopher, Hongliang Xin, and Suljo Linic. Visible-light-enhanced catalytic oxidation reactions on plasmonic silver nanostructures. *Nat. Chem.*, 3(6):467, 2011.

[6] Robert Charles Boutelle, Daniel Neuhauser, and Shimon Weiss. Far-field super-resolution detection of plasmonic near-fields. *ACS Nano*, 10(8):7955–7962, 2016.

[7] David Solis Jr, Aniruddha Paul, Jana Olson, Liane S Slaughter, Pattanawit Swanglap, Wei-Shun Chang, and Stephan Link. Turning the corner: Efficient energy transfer in bent plasmonic nanoparticle chain waveguides. *Nano Lett.*, 13(10):4779–4784, 2013.

[8] KR Catchpole and A Polman. Design principles for particle plasmon enhanced solar cells. *Appl. Phys. Lett.*, 93(19):191113, 2008.

[9] Surbhi Lal, Susan E Clare, and Naomi J Halas. Nanoshell-enabled photothermal cancer therapy: impending clinical impact. *Acc. Chem. Res.*, 41(12):1842–1851, 2008.

[10] Craig F. Bohren and Donald R. Huffman. *Absorption and Scattering of Light by Small Particles*. Wiley, 1998.

[11] Daniel Gall. Electron mean free path in elemental metals. *J. Appl. Phys.*, 119(8):085101, 2016.

[12] K Lance Kelly, Eduardo Coronado, Lin Lin Zhao, and George C Schatz. The optical properties of metal nanoparticles: the influence of size, shape, and dielectric environment, 2003.

[13] Robert C Boutelle, Yi Gao, Chris Arntsen, and Daniel Neuhauser. Nanodentures and mechanical electrodynamics: Three-dimensional relative orientation of plasmonic nanoarches from absorption spectra. *The Journal of Physical Chemistry C*, 117(18):9381–9385, 2013.

[14] Jonathan A Scholl, Ai Leen Koh, and Jennifer A Dionne. Quantum plasmon resonances of individual metallic nanoparticles. *Nature*, 483(7390):421, 2012.

[15] U Kreibig and L Genzel. Optical absorption of small metallic particles. *Surf. Sci.*, 156:678–700, 1985.

[16] Gustav Mie. Beiträge zur optik trüber medien, speziell kolloidaler metallösungen. *Ann. Phys.*, 330(3):377–445, 1908.

[17] Ardavan F. Oskooi and David Roundy andothers. Meep: A flexible free-software package for electromagnetic simulations by the fdtd method. *Comput. Phys. Commun.*, 181:687–702, 2010.

[18] Uwe Kreibig and Michael Vollmer. *Optical properties of metal clusters*, volume 25. Springer Science & Business Media, 2013.

[19] L Genzel, TP Martin, and U Kreibig. Dielectric function and plasma resonances of small metal particles. *Zeitschrift für Physik B Condensed Matter*, 21(4):339–346, 1975.

[20] K Lindfors, T Kalkbrenner, P Stoller, and V Sandoghdar. Detection and spectroscopy of gold nanoparticles using supercontinuum white light confocal microscopy. *Phys. Rev. Lett.*, 93(3):037401, 2004.

[21] Stéphane Berciaud, Laurent Cognet, Philippe Tamarat, and Brahim Lounis. Observation of intrinsic size effects in the optical response of individual gold nanoparticles. *Nano Lett.*, 5(3):515–518, 2005.

[22] Hongjian Liu, Bongjin Simon Mun, Geoff Thornton, Steven R Isaacs, Young-Seok Shon, D Frank Ogletree, and Miquel Salmeron. Electronic structure of ensembles of gold nanoparticles: Size and proximity effects. *Phys. Rev. B*, 72(15):155430, 2005.

[23] Roi Baer, Daniel Neuhauser, and Eran Rabani. Self-averaging stochastic kohn-sham density-functional theory. *Phys. Rev. Lett.*, 111:106402, 2013.

[24] Daniel Neuhauser, Yi Gao, Christopher Arntsen, Cyrus Karshenas, Eran Rabani, and Roi Baer. Breaking the theoretical scaling limit for predicting quasiparticle energies: The stochastic gw approach. *Phys. Rev. Lett.*, 113(7):076402, 2014. RBaer-Publication.

[25] Eran Rabani, Roi Baer, and Daniel Neuhauser. Time-dependent stochastic bethe-salpeter approach. *Phys. Rev. B*, 91(23):235302, 2015. RBaer-Publication.

[26] Yi Gao, Daniel Neuhauser, Roi Baer, and Eran Rabani. Sublinear scaling for time-dependent stochastic density functional theory. *J. Chem. Phys.*, 142(034106), 2015.

[27] A. S. Barnard. Modelling of nanoparticles: approaches to morphology and evolution. *Rep. Prog. Phys.*, 73:086502, 2010.

[28] A. S. Barnard. Direct comparison of kinetic and thermodynamic influences on gold nanomorphology. *Acc. Chem. Res.*, 45:1688–1697, 2012.

[29] John P. Perdew and Yue Wang. Accurate and simple analytic representation of the electron-gas correlation energy. *Phys. Rev. B*, 45(23):13244–13249, jun 1992.

[30] Luis J Mendoza Herrera, David Munetón Arboleda, Daniel C Schinca, and Lucía B Scaffardi. Determination of plasma frequency, damping constant, and size distribution from the complex dielectric function of noble metal nanoparticles. *J. Appl. Phys.*, 116(23):233105, 2014.

[31] Alexandre Vial and Thierry Laroche. Description of dispersion properties of metals by means of the critical points model and application to the study of resonant structures using the fdtd method. *J. Phys. D: Appl. Phys.*, 40(22):7152, 2007.

[32] Aleksandar D Rakić, Aleksandra B Djurišić, Jovan M Elazar, and Marian L Majewski. Optical properties of metallic films for vertical-cavity optoelectronic devices. *Appl. Opt.*, 37(22):5271–5283, 1998.

[33] Jonathan A Scholl, Ai Leen Koh, and Jennifer A Dionne. Quantum plasmon resonances of individual metallic nanoparticles. *Nature*, 483(7390):421, 2012.

[34] WMH Sachtler, GJH Dorgelo, and AA Holscher. The work function of gold. *Surf. Sci.*, 5(2):221–229, 1966.

[35] Kenneth Price, Rainer M Storn, and Jouni A Lampinen. *Differential evolution: a practical approach to global optimization*. Springer Science & Business Media, 2006.

[36] John Towns, Timothy Cockerill, Maytal Dahan, Ian Foster, Kelly Gaither, Andrew Grimshaw, Victor Hazlewood, Scott Lathrop, Dave Lifka, Gregory D Peterson, et al. Xsede: accelerating scientific discovery. *Comput. Sci. Eng.*, 16(5):62–74, 2014.